

Theory of Spin-Resolved Auger-Electron Spectroscopy from Ferromagnetic 3d-Transition Metals

T. Wegner,* M. Potthoff, and W. Nolting

*Theoretische Festkörperphysik, Institut für Physik,
Humboldt-Universität zu Berlin, Invalidenstraße 110, 10115 Berlin, Germany*

CVV Auger electron spectra are calculated for a multi-band Hubbard model including correlations among the valence electrons as well as correlations between core and valence electrons. The interest is focused on the ferromagnetic 3d-transition metals. The Auger line shape is calculated from a three-particle Green function. A realistic one-particle input is taken from tight-binding band-structure calculations. Within a diagrammatic approach we can distinguish between the *direct* correlations among those electrons participating in the Auger process and the *indirect* correlations in the rest system. The indirect correlations are treated within second-order perturbation theory for the self-energy. The direct correlations are treated using the valence-valence ladder approximation and the first-order perturbation theory with respect to valence-valence and core-valence interactions. The theory is evaluated numerically for ferromagnetic Ni. We discuss the spin-resolved quasi-particle band structure and the Auger spectra and investigate the influence of the core hole.

I. INTRODUCTION

Auger-electron spectroscopy (AES) and the complementary appearance-potential spectroscopy (APS) have become valuable tools for investigating the electronic structure of solids and solid surfaces^{1,2,3,4,5,6,7,8}. They represent highly element specific and non-destructive methods with a comparatively simple experimental set up. The Auger line shape from a core-valence-valence (CVV) process yields information on the occupied part of the valence band, while the APS provides insight into the unoccupied valence states. However, much effort has been spent on the detailed interpretation of the spectra. Lander⁹ suggested that the spectrum obtained by AES (APS) is given as the self-convolution of the occupied (unoccupied) valence density of states (DOS). On the other hand, Powell¹⁰ discovered the CVV Auger line shape of Ag to behave “anomalously” in the sense of Lander’s self-convolution model. These anomalous features are by now well known to be caused by correlation effects dominating the electronic properties of various solids. Therefore, AES (APS) seems to be a useful technique to study electron-correlation effects, but it is doubtful whether it is able to compete with one-particle spectroscopies, such as photoemission (inverse photoemission), in deriving the DOS by deconvolution.

In the theoretical treatment of the CVV Auger process, there are mainly two problems. The first one is to take into account the correlation effects. Here one may distinguish between the *direct* and *indirect* correlations. The direct correlations describe the correlations of those electrons which participate in the Auger process. They are responsible for the most prominent effects in the Auger line shape as compared to the self-convolution. On the other hand, the indirect correlations among the electrons in the rest system manifest themselves in the quasi-particle density of states (QDOS) as a renormalisation of the one-particle DOS.

The second problem is the calculation of the transition-

matrix elements for the Auger process as well as the scattering of the outgoing Auger electron (cf. Refs. 11,12). These effects will (slightly) modify the bare line shape and may become important for a refined interpretation of experimental data. Within the present paper, however, we set aside this second problem and like to concentrate on electron-correlation effects in AES from ferromagnetic 3d-transition metals.

Within the framework of the single-band Hubbard model, correlation effects can be treated exactly for systems with completely filled or empty bands, as was first shown by Cini and Sawatzky^{13,14,15}. The generalisation to the case of degenerate bands was introduced in Ref. 16 and further analysed in Ref. 17, for example. These results may also be extended to include the core-valence interaction¹⁸.

Considering the more general case of partially filled bands introduces several complications concerning the indirect as well as the direct correlations. For the indirect valence-valence correlations there is a number of approximation schemes applicable to a multi-band Hubbard model. A method which reproduces the experimentally observed Curie temperature quite well, especially for Ni, is the spectral density approach^{19,20}. Other approaches are, for example, the generalisation of the single-band modified perturbation theory²¹ to the multi-band model^{22,23} and Quantum-Monte-Carlo simulations²⁴ in connection with the dynamical mean-field theory²⁵. However, these methods suffer from some necessary restrictions concerning the completeness of the Coulomb-matrix. This is not the case for the fluctuation exchange²⁶ and the Hubbard I approximation²³, for example. For a more detailed discussion on the indirect valence-valence correlations see Ref. 23.

For the treatment of the direct correlations, one has the exact-diagonalisation method²⁷ for small systems and the equation-of-motion method^{28,29} with its in general uncontrolled termination of the hierarchy of the equations of motion. Another approximate solution is the valence-valence ladder (VV ladder) approximation^{30,31,32,33,34}

and its generalisation to include the core-valence interaction^{35,36,37,38} (CVV ladder). In particular one has to account for the broken translational symmetry in the initial state of AES, caused by the presence of the core hole and its screening due to the valence electrons. In the final state this interaction is responsible for the sudden response of the valence electrons due to the destruction of the core hole. In the limit of completely filled or empty bands the ladder approximations recover the above-mentioned exact solution.

Here the interaction strength is taken as the control parameter, which is correct in the weak-coupling regime. We are aware that this method has restrictions for the 3d-transition metals. However, in this work we prefer a common treatment of one-particle spectroscopies (photoemission and inverse photoemission) and two-particle spectroscopies like AES. To be concrete, we will use the second-order perturbation theory around the Hartree-Fock solution^{39,40,41} for the indirect valence-valence correlations. The direct correlations will be treated by applying two different methods, i. e. the VV ladder approximation and the first-order perturbation theory in the valence-valence and core-valence interaction.

Within this approach it is possible to include a realistic one-particle input taken from tight-binding band-structure calculations. We do not only account for the degeneracy of the 3d-band but also for the hybridisation with the 4s and 4p states. The theory is formulated and evaluated for a non-orthogonal basis set where the states can be distinguished by the angular momentum quantum number and the cubic harmonic index. This facilitates the interpretation of the resulting spectra. Furthermore, we do not restrict ourselves to correlations among the final-state holes only and include core-hole effects from the very beginning. This implies the necessity for a proper treatment of the initial state where the core-hole screening breaks the translational symmetry. The theory is implemented numerically and evaluated for ferromagnetic Ni.

The paper is organised as follows. In the next section we will introduce the model under consideration. In section III we give the expression for the Auger intensity. Section IV concentrates on the indirect and section V on the direct correlations. Finally, section VI concludes the paper. Some details concerning the non-orthogonal basis set are given in the appendix A.

II. MODEL

The Hamiltonian $\mathcal{H} = H_0 - \mu N + H_I$ is decomposed into a one-particle part $H_0 - \mu N$ and an interaction part H_I . N is the operator for the particle number. The one-particle part describes non-interacting valence and core electrons:

$$H_0 - \mu N = \sum_{\substack{i,i',\sigma, \\ L,L'}} \left(t_{ii'}^{LL'} - \mu S_{ii'}^{LL'} \right) c_{iL\sigma}^\dagger c_{i'L'\sigma}$$

$$+ \sum_{i,\sigma} (\epsilon_c - \mu) b_{i\sigma}^\dagger b_{i\sigma} \quad (1)$$

The index i refers to lattice sites, σ is the spin-index ($\sigma = \uparrow, \downarrow$), $L = \{l, m\}$ is the orbital index with angular momentum quantum number l and cubic harmonic index m . $c_{iL\sigma}^\dagger$ ($c_{iL\sigma}$) denotes the creation (annihilation) operator of a valence electron at the lattice site i with spin σ and orbital index L while $b_{i\sigma}^\dagger$ ($b_{i\sigma}$) creates (annihilates) a core electron. The core states are assumed to be non-degenerate and dispersionless with the one-particle energy ϵ_c well below the chemical potential μ . The hopping integrals $t_{ii'}^{LL'}$

$$\langle iL\sigma | h^{\text{BS}} | i'L'\sigma' \rangle = t_{ii'}^{LL'} \delta_{\sigma\sigma'} \quad (2)$$

(h^{BS} denotes the Hamiltonian of the tight-binding band-structure calculation) are taken from Ref. 42 as well as the overlap integrals $S_{ii'}^{LL'}$

$$\langle iL\sigma | i'L'\sigma' \rangle = S_{ii'}^{LL'} \delta_{\sigma\sigma'} . \quad (3)$$

$t_{ii'}^{LL'}$ and $S_{ii'}^{LL'}$ refer to a non-orthogonal basis set (see appendix A). Contrary to an orthonormal basis set (where the overlap matrix is replaced by $\delta_{ii'} \delta_{LL'}$), the basis states under consideration can be characterised by the orbital index $L = \{l, m\}$. The construction operators likewise refer to the non-orthogonal basis and satisfy the following anti-commutation rules:

$$\begin{aligned} [c_{iL\sigma}, c_{i'L'\sigma'}]_+ &= 0 \\ [c_{iL\sigma}, c_{i'L'\sigma'}^\dagger]_+ &= (S^{-1})_{ii'}^{LL'} \delta_{\sigma\sigma'} . \end{aligned} \quad (4)$$

It should be noted that the action of the creation operator on the vacuum state $c_{iL\sigma}^\dagger |0\rangle$, in general, does not yield $|iL\sigma\rangle$ (see Eq. (A.5) of the appendix A).

To describe the correlations among the valence electrons (VV) as well as the correlations between valence and core electrons (CV) the interaction consists of two parts

$$\begin{aligned} H_I &= \frac{1}{2} \sum_{\substack{i,\sigma,\sigma', \\ L_1,\dots,L_4}} U_{L_1 L_2 L_4 L_3} c_{iL_1\sigma}^\dagger c_{iL_2\sigma'}^\dagger c_{iL_3\sigma'} c_{iL_4\sigma} - H_{\text{dc}}^{\text{VV}} \\ &+ \sum_{i,\sigma,\sigma',L} U_L^c n_{iL\sigma} n_{i\sigma'}^c - H_{\text{dc}}^{\text{CV}} . \end{aligned} \quad (5)$$

Here the occupation number operator for valence electrons is $n_{iL\sigma} = c_{iL\sigma}^\dagger c_{iL\sigma}$ and for core electrons $n_{i\sigma}^c = b_{i\sigma}^\dagger b_{i\sigma}$. Assuming a strong screening of the Coulomb interaction, the interaction part is taken to be purely local. $U_{L_1 L_2 L_4 L_3}$ are the on-site Coulomb-matrix elements for the valence electrons.

The electronic structure of the 3d-transition metals may be understood considering mainly two types of electronic orbitals: The 4s- and 4p-states which form broad free-electron like bands. They should be well described by

the band-structure calculation. The other group are the well localised 3d-states which in the solid form relatively narrow bands positioned around the Fermi energy. The localised nature of the 3d-electrons gives rise to important dynamic 3d-3d correlation effects which are believed to be responsible e. g. for the magnetic behaviour of the 3d-transition metals. These correlations may not be adequately taken into account within a mean-field picture. We thus treat them separately.

Exploiting atomic symmetries, one is able to express all remaining Coulomb-matrix elements for the 3d-electrons in terms of three effective Slater integrals^{43,44} (F^0 , F^2 , F^4) only. These integrals are connected to averaged values for direct

$$U = \frac{1}{25} \sum_{L,L'} U_{LL'LL'} = F^0 \quad (6)$$

and exchange interaction terms

$$J = \frac{1}{20} \sum_{L \neq L'} U_{LL'L'L} = \frac{F^2 + F^4}{14}. \quad (7)$$

For 3d-elements one has to a good accuracy the ratio $F^2/F^4 \approx 0.625$ ⁴⁴ to be that of free ions⁴³. U and J are treated as free parameters to be fixed by comparison with experimental results (see section IV).

The CV interaction part is necessary to describe the core hole effects in AES. U_L^c in equation (5) are the Coulomb-matrix elements between the valence and the core electrons which can be fixed by assuming complete screening of the core hole by the valence electrons (see section IV). To avoid a double counting of interactions, we subtract the correction $H_{dc}^{VV(CV)}$ which is to a good approximation the Hartree-Fock part of the respective interaction term⁴⁴.

III. AUGER INTENSITY

The Auger process can be divided into two subprocesses. The first one is the creation of a core hole with spin σ_c at the lattice site i_c by absorbing an x-ray quantum for example. The second subprocess is the radiationless decay of the core hole via ejecting an Auger electron with spin σ and momentum \mathbf{k} . Provided that the life time of the core hole is large compared to typical relaxation times of the valence electrons in the presence of the core hole, the two subprocesses become independent from each other³ (two-step model). This implies the absence of any decay term in the Hamiltonian. Consequently $n_{i_c\sigma_c}^c$ is a good quantum number, $[H, n_{i_c\sigma_c}^c]_- = 0$. We can concentrate on the second subprocess. Within the two-step model the initial state for the Auger transition process is the ground state within the subspace \mathcal{H}^e of the Hilbert space \mathcal{H} that is built up by all many-body states with $n_{i_c\sigma_c}^c = 0$. To perform thermodynamic averages in practice, one has to take into account this restriction by introducing an additional Lagrange parameter.

The transition process itself is described by the transition operator³⁵

$$T_{\mathbf{k}\sigma\sigma_c} = \sum_{L_1, L_2} M_{i_c\mathbf{k}}^{L_1 L_2} c_{i_c L_1 \sigma}^\dagger c_{i_c L_2 \sigma_c}^\dagger b_{i_c \sigma_c}. \quad (8)$$

\mathbf{k} and σ denote the quantum-numbers of the Auger electron, σ_c the spin of the core state involved. The (intra-atomic) Auger-matrix elements are given by

$$\begin{aligned} M_{i_c\mathbf{k}}^{L_1 L_2} &= \langle i_c L_1, i_c L_2 | H_{\text{Coulomb}} | \mathbf{k}, i_c \rangle \\ &\propto \iint d^3 r_1 d^3 r_2 \bar{\Psi}_{L_1}(\mathbf{r}_1 - \mathbf{R}_{i_c}) \bar{\Psi}_{L_2}(\mathbf{r}_2 - \mathbf{R}_{i_c}) \\ &\quad \times \frac{1}{|\mathbf{r}_1 - \mathbf{r}_2|} \Phi_{\mathbf{k}}(\mathbf{r}_1) \phi(\mathbf{r}_2 - \mathbf{R}_{i_c}) \end{aligned} \quad (9)$$

where Ψ is the valence orbital, Φ the one-particle wavefunction of the Auger-electron and ϕ the core state. The bar denotes complex conjugation.

Following Ref. 35 we consider the (retarded) three-particle Green function, relevant for AES, which is defined as (with the abbreviation $\mathbf{L} = (L_1, L_2)$ and $\mathbf{L}' = (L'_1, L'_2)$)

$$\begin{aligned} G_{\mathbf{k}\sigma\sigma_c}^{(3)}(E) &= \langle \langle T_{\mathbf{k}\sigma\sigma_c}^\dagger; T_{\mathbf{k}\sigma\sigma_c} \rangle \rangle_E \\ &= \sum_{\mathbf{L}, \mathbf{L}'} \bar{M}_{i_c\mathbf{k}}^{\mathbf{L}} G_{i_c\sigma\sigma_c}^{(3), \mathbf{L}\mathbf{L}'}(E) M_{i_c\mathbf{k}}^{\mathbf{L}'} \end{aligned} \quad (10)$$

with

$$G_{i_c\sigma\sigma_c}^{(3), \mathbf{L}\mathbf{L}'}(E) = \langle \langle b_{i_c\sigma_c}^\dagger c_{i_c L_2 \sigma_c} c_{i_c L_1 \sigma}; c_{i_c L'_1 \sigma}^\dagger c_{i_c L'_2 \sigma_c}^\dagger b_{i_c \sigma_c} \rangle \rangle_E. \quad (11)$$

$\langle \langle \cdot; \cdot \rangle \rangle_E$ refers to Zubarev Green functions^{45,46}. The AES intensity is then mainly given by the three-particle spectral-density $A_{\mathbf{k}\sigma\sigma_c}^{(3)}(E) = -(1/\pi) \Im G_{\mathbf{k}\sigma\sigma_c}^{(3)}(E)$:

$$I_{\mathbf{k}\sigma\sigma_c}(E + \epsilon_c - \mu) \propto \delta(E - E(\mathbf{k})) A_{\mathbf{k}\sigma\sigma_c}^{(3)}(E). \quad (12)$$

Here $E(\mathbf{k})$ is the dispersion of the Auger-electron.

In general the three-particle Green function will be a (complicated) functional of one-particle Green functions. This functional represents the direct correlations. In the following we concentrate on the indirect correlations first, i. e. on the determination of the relevant one-particle Green functions.

IV. INDIRECT CORRELATIONS

A. Valence-band interaction

We consider the (retarded) one-particle valence-band Green-function $\langle \langle c_{iL\sigma}; c_{i'L'\sigma}^\dagger \rangle \rangle_E$. Using a matrix notation with respect to the orbital index $L = \{l, m\}$

$$(\mathbf{X}_{ii'})^{LL'} = X_{ii'}^{LL'} \quad (13)$$

and defining a lattice-Fourier transformation

$$\mathbf{X}_{\mathbf{k}} = \frac{1}{N_s} \sum_{i,i'} e^{-i\mathbf{k}(\mathbf{R}_i - \mathbf{R}_{i'})} \mathbf{X}_{ii'}, \quad (14)$$

where N_s is the number of lattice sites, we get Dyson's equation in the form

$$\mathbf{G}_{ii'\sigma}(E) = \frac{1}{N_s} \sum_{\mathbf{k}} \frac{e^{i\mathbf{k}(\mathbf{R}_i - \mathbf{R}_{i'})}}{(E + \mu) \mathbf{S}_{\mathbf{k}} - \mathbf{t}_{\mathbf{k}} - \mathbf{\Sigma}_{\mathbf{k}\sigma}(E)}. \quad (15)$$

Here the matrices $\mathbf{t}_{\mathbf{k}}$ and $\mathbf{S}_{\mathbf{k}}$ are the Fourier-transformed hopping and overlap integrals of Eqs. (2) and (3), respectively. $\mathbf{\Sigma}_{\mathbf{k}\sigma}(E)$ is the self-energy. The one-particle spectral density is given by

$$\mathbf{A}_{ii'\sigma}(E) = -\frac{1}{\pi} \Im \mathbf{G}_{ii'\sigma}(E + i0^+). \quad (16)$$

The on-site terms of the spectral density are diagonal in the orbital index as a consequence of lattice symmetries, and we have for the orbital resolved QDOS

$$\rho_{\sigma}^L(E) = A_{ii\sigma}^{LL}(E - \mu) \quad (17)$$

where we dropped the site index. The total QDOS is obtained via

$$\rho_{\sigma}(E) = \sum_{i'} \text{Tr} \{ \mathbf{S}_{ii'} \mathbf{A}_{i'i\sigma}(E - \mu) \}. \quad (18)$$

To calculate the self-energy, we use a standard approximation scheme, the second order perturbation theory around the Hartree-Fock solution^{39,40,41,47,48} (SOPT-HF). It is known from the single-band Hubbard model that the non-local terms of the SOPT-HF self-energy rapidly decrease with increasing number of shells taken into account^{47,48}. Furthermore, due to the band degeneracy there is a much weaker \mathbf{k} -dependence of the SOPT-HF self-energy compared to the single-band case⁴¹. We may thus employ the local approximation

$$\Sigma_{ii'\sigma}^{LL'}(E) \approx \Sigma_{ii\sigma}^{LL'}(E) \delta_{ii'} = \Sigma_{\sigma}^L(E) \delta_{LL'} \delta_{ii'} \quad (19)$$

As for the on-site Green function, lattice symmetries require the on-site self-energy to be diagonal in the orbital index.

The Hartree-Fock (HF) contribution to the self-energy reads as

$$\Sigma_{\sigma}^{(\text{HF}),L} = \sum_{L_1} \left\{ U_{LL_1LL_1} \left(n_{-\sigma}^{L_1} - n_{-\sigma}^{(0)L_1} \right) + \left(U_{LL_1LL_1} - U_{LL_1L_1L} \right) \left(n_{\sigma}^{L_1} - n_{\sigma}^{(0)L_1} \right) \right\} \quad (20)$$

where $n_{\sigma}^L = \langle n_{iL\sigma} \rangle$ denotes the expectation value in the full model and $n_{\sigma}^{(0)L}$ the expectation value of the band-structure calculation that stems from the double counting correction in equation (5). Approximating the self-energy by $\Sigma_{\sigma}^{(\text{HF}),L}$, corresponds to the LDA+ U approach⁴⁴. Here we additionally include the next order in

the interaction. The second-order contribution (SOC) to the self-energy reads as

$$\begin{aligned} \Sigma_{\sigma}^{(\text{SOC}),L}(E) &= \iiint \frac{dx dy dz}{E - x + y - z} \\ &\times (f_{-}(x)f_{-}(-y)f_{-}(z) + f_{-}(-x)f_{-}(y)f_{-}(-z)) \\ &\times \sum_{L_1, L_2, L_3} U_{LL_1L_3L_2} \tilde{\rho}_{\sigma}^{L_3}(x) \left\{ U_{L_3L_2LL_1} \tilde{\rho}_{-\sigma}^{L_1}(y) \tilde{\rho}_{-\sigma}^{L_2}(z) \right. \\ &\quad \left. + (U_{L_3L_2LL_1} - U_{L_3L_2L_1L}) \tilde{\rho}_{\sigma}^{L_1}(y) \tilde{\rho}_{\sigma}^{L_2}(z) \right\} \end{aligned} \quad (21)$$

with the Fermi function $f_{-}(E) = (e^{\beta E} + 1)^{-1}$ and where the local HF spectral-density $\tilde{\rho}_{\sigma}^L(E) = A_{ii\sigma}^{(\text{HF}),LL}(E)$ is obtained by using the HF self-energy (20) in equation (15). The SOPT-HF self-energy

$$\mathbf{\Sigma}_{\sigma}(E) = \mathbf{\Sigma}_{\sigma}^{(\text{HF})} + \mathbf{\Sigma}_{\sigma}^{(\text{SOC})}(E) \quad (22)$$

determines the full Green function via equation (15).

B. Core-valence interaction

1. Valence-band Green function

Let us now focus on the core hole screening in the initial state for AES. The CV interaction and the presence of the core hole introduce an additional (Hartree-like) term

$$\Sigma_{i\sigma}^{(\text{CV},e),L} = -\delta_{ii_c} U_L^c \quad (23)$$

to the valence-band self-energy which breaks the translational symmetry. This term represents the core-hole potential at the lattice site i_c where the core hole was created (the superscript ‘‘e’’ indicates averaging in the restricted Hilbert-space \mathcal{H}^e ; see section III). It is responsible for the screening. The valence-band self-energy in the presence of the core hole then reads

$$\Sigma_{i\sigma}^e(E) = \Sigma_{i\sigma}^{(\text{VV},e)}(E) + \Sigma_{i\sigma}^{(\text{CV},e)}. \quad (24)$$

$\Sigma_{\sigma}^{(\text{VV},e)}(E)$ incorporates the VV-correlation effects and has the same structure as the self-energy (22) for the translational invariant system. But in contrast to its translational invariant counterpart, $\Sigma_{\sigma}^{(\text{VV},e)}(E)$ is defined in terms of the Green functions in the presence of the core hole.

The valence band Green function $\mathbf{G}_{ii'\sigma}^e(E)$ in the presence of the core hole can be obtained by using Dyson's equation in the form

$$\begin{aligned} \mathbf{G}_{ii'\sigma}^e(E) &= \mathbf{G}_{ii'\sigma}(E) \\ &+ \sum_j \mathbf{G}_{ij\sigma}(E) (\mathbf{\Sigma}_{j\sigma}^e(E) - \mathbf{\Sigma}_{\sigma}(E)) \mathbf{G}_{ji'\sigma}^e(E). \end{aligned} \quad (25)$$

In general $\Sigma_{i\sigma}^e(E) - \Sigma_{\sigma}(E) \neq 0$ for a certain number of shells around the core-hole site because the VV-correlation effects depend on the occupation numbers,

which as a consequence of the screening locally differ from the translational invariant ones. In the following we assume complete screening, i. e. charge neutrality at the site i_c , which is reasonable especially for 3d-transition metals because the screening time scale is small compared to the life-time of the core hole²⁷. This implies $\Sigma_{i\sigma}^e(E) - \Sigma_\sigma(E)$ to be small for all sites i except for $i = i_c$. Neglecting the terms for $i \neq i_c$ one can solve equation (25)

$$\mathbf{G}_{ii'\sigma}^e(E) = \mathbf{G}_{ii'\sigma}(E) + \mathbf{G}_{i_c\sigma}(E) \quad (26)$$

$$\times \left((\Sigma_{i_c\sigma}^e(E) - \Sigma_\sigma(E))^{-1} - \mathbf{G}_{i_c\sigma}(E) \right)^{-1} \mathbf{G}_{i_c\sigma}(E).$$

For $i = i' = i_c$ one obtains the local screened Green-function at the core-hole site:

$$\mathbf{G}_{i_c\sigma}^e(E) = \frac{1}{\mathbf{G}_{i_c\sigma}^{-1}(E) - (\Sigma_{i_c\sigma}^e(E) - \Sigma_\sigma(E))}. \quad (27)$$

The assumption of complete screening will be utilised as condition to fix the CV-interaction parameter, which is taken to be the same for s-, p- and d-orbitals ($U_L^c \equiv U_c$).

2. Core Green function

To take into account the CV interaction for the core Green function

$$g_{i_c\sigma_c}(E) = \langle\langle b_{i_c\sigma_c}; b_{i_c\sigma_c}^\dagger \rangle\rangle_E \quad (28)$$

$$= \frac{1}{E + \mu - \epsilon_c - \Sigma_{i_c\sigma_c}^c(E)}$$

one may calculate the core self-energy $\Sigma_{i_c\sigma_c}^c(E)$ using e. g. the SOPT-HF in the same way as for the valence-band Green function. On the other hand it is believed that the core states are influenced by other and presumably more important effects, such as life-time effects³. In fact, the core spectral density obtained within SOPT-HF turns out to be dominated by a delta-peak that is shifted by about 1 eV below $\epsilon_c - \mu$. This does not affect the Auger line shape. Therefore, we assume for convenience the core self-energy to be zero. The spectral density becomes

$$a_{i_c\sigma_c}(E) = -\frac{1}{\pi} \Im g_{i_c\sigma_c}(E + i0^+) = \delta(E + \mu - \epsilon_c). \quad (29)$$

C. Results for Ni

Before we discuss the results for fcc-Ni, we like to make a short remark concerning the numerical evaluation of the theory. The \mathbf{k} -sum for the local Green function in equation (15) was performed on a mesh of 240 \mathbf{k} -points within the irreducible part of the Brillouin zone using the tetrahedron method⁴⁹ generalised to complex band structures, similar to that presented in Ref. 50. The evaluation of the total QDOS (18) as well as the QDOS in the presence of the core hole was done in \mathbf{k} -space. For

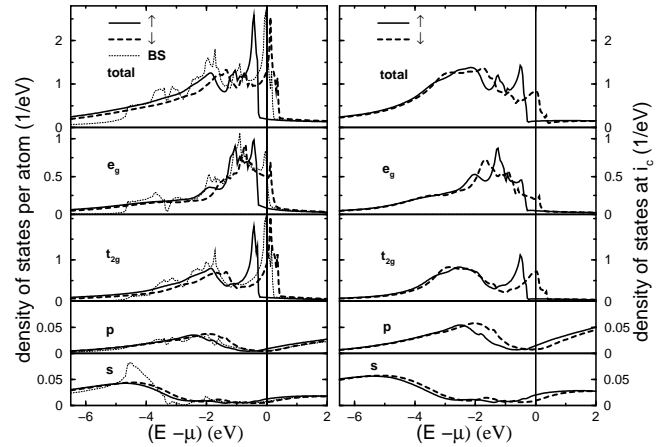


FIG. 1: Spin-resolved QDOS per atom for s-, p-, t_{2g} -, e_g -states and total QDOS for $U = 2.47$ eV, $J = 0.5$ eV and $T = 0$ K. Left: unscreened QDOS. Thin dotted line: tight-binding band-structure calculation⁴² for paramagnetic Ni. Right: screened QDOS at the site i_c in the presence of the core hole, $U_c = 1.81$ eV.

the latter, equation (25) has to be used to perform the Fourier transformation.

The effective Slater integrals or, equivalently, the averaged direct and exchange interaction parameters are chosen as $U = 2.47$ eV and $J = 0.5$ eV. This leads to a calculated magnetic moment per atom of $m = 0.56 \mu_B$ at $T = 0$ K which is the same as the measured moment⁵¹. With the ratio $J/U \approx 0.2$ we assume a typical value for the late 3d transition metals. The values given in the literature, for instance $U = 3.7$ eV, $J = 0.27$ eV⁴¹ and $U = 2.97$ eV, $J = 0.8$ eV⁵², are of the same order of magnitude but slightly overestimate the magnetic moment within the present theory. The “free” DOS, used as starting point for our theory is shown on the left of figure 1 (thin dotted line) and corresponds to tight binding band structure calculations⁴² for paramagnetic fcc-Ni.

The left-hand side of figure 1 shows the QDOS per atom for the model parameters given above. As is known from the experiment, Ni is a strong ferromagnet, i. e. the majority-spin states are fully occupied. The renormalisation effects of the a priori uncorrelated s- and p-states seen in figure 1 can be traced back to the hybridisation with the d-states.

Taking into account the presence of the core hole and following the procedure to fix the CV interaction parameter as described above (charge neutrality), leads to $U_c = 1.81$ eV. The corresponding “screened” QDOS is plotted on the right-hand side of figure 1. The structure has changed remarkably. Spectral weight of the d-electrons from the upper band edge is transferred to lower energies, the s- and p-states are more populated, too. The screened magnetic moment at the site i_c ($m_{i_c}^e = 0.1 \mu_B$ at $T = 0$ K) is considerably decreased since the local oc-

cupation is increased (see also figure 3).

The left side of figure 2 shows the self-energy $\Sigma_\sigma^L(E)$. Within an energy range of about 1 eV above and below $E = 0$ eV one has $\Im\Sigma_\sigma^L(E) \propto E^2$. Thus we have well-defined quasi-particles at the Fermi energy and their weight

$$z_\sigma^L = \left| 1 - \frac{\partial \Re\Sigma_\sigma^L(E=0)}{\partial E} \right|^{-1} \quad (30)$$

is 0.887 for the $t_{2g}\text{-}\uparrow$ -states and 0.893 for $t_{2g}\text{-}\downarrow$ -states. For e_g -states we find 0.878 and 0.883, respectively. For energies above -2 eV, where one finds clearly distinguishable structures, a significant band-narrowing caused by the real part of the self-energy is observed. While the imaginary part of the self-energy leads to strong damping effects in the QDOS (figure 1, l. h. s.) for energies below -2 eV. About -6 eV below the Fermi energy where one expects the ‘‘Ni-6-eV-satellite’’^{53,54,55} we find the largest damping effects. However, we do not find the correlation-induced 6 eV satellite. This is not surprising by applying the SOPT-HF or any other finite-order perturbational approach^{30,56,57}. For different interaction parameters (larger U , smaller J) a small shoulder in the QDOS of the d-states is visible as was also mentioned in Ref. 40. On the right-hand side of figure 2 the self-energy in the presence of the core hole $\Sigma_{i_c\sigma}^{e,L}(E)$ is plotted. Again there are well-defined quasi-particles, but with an enhanced weight compared to the case where the core hole is absent ($z_{i_c\uparrow}^{t_{2g}} = 0.940$, $z_{i_c\downarrow}^{t_{2g}} = 0.934$, $z_{i_c\uparrow}^{e_g} = 0.937$, $z_{i_c\downarrow}^{e_g} = 0.936$). The screened case behaves less correlated than the unscreened case since here one is closer to the limit of completely filled bands.

Finally, we show the local magnetic moment per atom as a function of temperature in figure 3. The magnetisation curves (figure 3, l. h. s.) have a Brillouin-function-like form, except for the e_g -magnetisation which shows up a maximum at $T \approx 1100$ K. This can be traced back to a transfer of charge carriers from the e_g -orbitals to the t_{2g} -orbitals with increasing temperature.

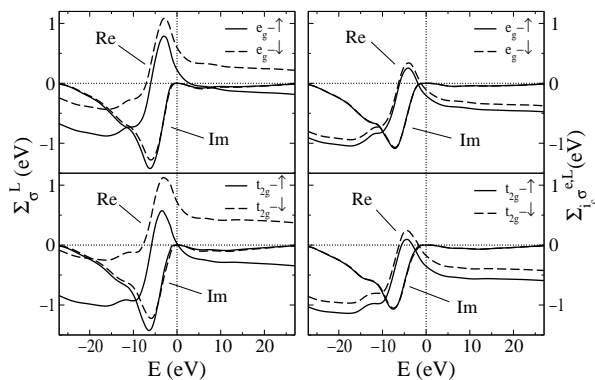


FIG. 2: Real and imaginary part of the self-energy. Left: for the translational invariant system ($\Sigma_\sigma^L(E)$). Right: for the system in the presence of the core hole ($\Sigma_{i_c\sigma}^{e,L}(E)$)

Because Ni is a strong ferromagnet the charge-carrier transfer leads to an increase of the e_g -magnetisation. Contrary, the t_{2g} -magnetisation is decreased in addition to the usual temperature-induced depolarisation. This leads to a temperature-dependent increase of the ratio $m_{e_g}/(m_{t_{2g}} + m_{e_g})$ as it is known from polarised neutron-scattering experiments^{58,59}. For $T = 0$ K this ratio is 0.20 and in good agreement with the measured value of 0.19^{58,59}. As is observed experimentally, the s- and p-states couple antiferromagnetically to the d-states^{58,59}. The Curie temperature turns out to be $T_C = 1655$ K and is thereby about a factor 2.6 larger than the measured value of 624 K⁶⁰. The large value for T_C is probably due to the mean-field character of the SOPT-HF. Note, however, that a simple LDA+ U (HF) calculation for the same parameters U and J yields a $T = 0$ magnetisation $0.57 \mu_B$ and a Curie temperature of approximately 2500 K.

The local moment at the site i_c as function of temperature is shown on the right-hand side of figure 3. Its d-contribution is strongly reduced compared to the unscreened case while the s- and p-moment is increased. The strong reduction of the total magnetic moment will influence the spin polarisation of AES, since the ‘‘screened’’ QDOS enters the Auger Green function 10. Note that the total magnetisation has to be calculated using equation (18), incorporating hybridisation with delocalised states.

V. DIRECT CORRELATIONS

To express the Auger intensity as a functional of the one-particle Green functions we consider the diagrammatic expansion of the three-particle Green function $G_{i_c\sigma\sigma_c}^{(3),\mathbf{L}\mathbf{L}'}(E)$ ($\mathbf{L} = (L_1, L_2)$). Here we can restrict ourselves to the direct diagrams and incorporate the exchange diagrams by introducing ‘‘direct’’ ($D_{i_c\mathbf{k}}^{\mathbf{L}} = M_{i_c\mathbf{k}}^{L_1L_2}$) and ‘‘exchange’’ Auger matrix elements ($E_{i_c\mathbf{k}}^{\mathbf{L}} = M_{i_c\mathbf{k}}^{L_2L_1}$). The Auger intensity then reads as

$$I_{\mathbf{k}\sigma\sigma_c}(E + \epsilon_c - \mu) \propto \delta(E - E(\mathbf{k})) \sum_{\mathbf{L}, \mathbf{L}'} \left(\overline{D}_{i_c\mathbf{k}}^{\mathbf{L}} - \delta_{\sigma\sigma_c} \overline{E}_{i_c\mathbf{k}}^{\mathbf{L}} \right) A_{i_c\sigma\sigma_c}^{(3),\mathbf{L}\mathbf{L}'}(E) D_{i_c\mathbf{k}}^{\mathbf{L}'} \quad (31)$$

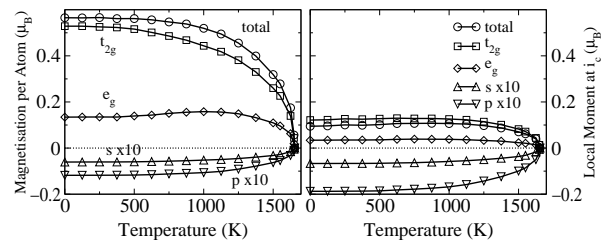


FIG. 3: Left: magnetisation as function of temperature. Right: local moment as function of temperature in the presence of the core hole.

The Auger matrix elements are taken to be constant. Following Ref. 12 we set:

$$M_{i_c \mathbf{k}}^{L_1 L_2} = \begin{cases} 1 & \text{for } L_1 \leq L_2 \\ -1 & \text{for } L_1 > L_2. \end{cases} \quad (32)$$

We thereby account for the singlet contributions, i. e. the holes in the final state have opposite spin ($\sigma = -\sigma_c$), as well as for the triplet contributions ($\sigma = \sigma_c$) to the Auger intensity. The triplet contributions would be ignored if the Auger matrix elements were chosen to be symmetric in the orbital index ($M_{i_c \mathbf{k}}^{L_1 L_2} = M_{i_c \mathbf{k}}^{L_2 L_1}$) because the transition operator then vanishes, as can be seen from equation (8).

A. VV ladder approximation

We consider two different approximation schemes for the treatment of the direct correlations. In the first approach, following Refs. 30,31,32,33,34 we neglect the direct CV correlations and treat the direct VV correlations by means of the VV ladder approximation, which becomes exact in the limit of completely filled or empty bands. A typical diagram contributing to the VV ladder is shown in figure 4. The solid lines represent the renormalised one-particle propagators of the valence-band while the wiggly line is the one-particle core-propagator. The dashed line corresponds to the VV interaction. Summing up all diagrams of this kind, yields the VV ladder approximation. The three-particle spectral density is given by

$$\begin{aligned} A_{i_c \sigma \sigma_c}^{(3), \mathbf{L} \mathbf{L}'}(E) &= \int dE' A_{i_c \sigma \sigma_c}^{(2), \mathbf{L} \mathbf{L}'}(E + E') \\ &\quad \times a_{i_c \sigma_c}(E') f_+(E + E') \\ &\stackrel{(29)}{=} A_{i_c \sigma \sigma_c}^{(2), \mathbf{L} \mathbf{L}'}(E + \epsilon_c - \mu) f_+(E + \epsilon_c - \mu) \end{aligned} \quad (33)$$

where $f_+(E) = (e^{\beta E} - 1)^{-1}$ is the Bose function. The two-particle valence-band spectral density $A_{i_c \sigma \sigma_c}^{(2), \mathbf{L} \mathbf{L}'}(E)$ is obtained from the corresponding two-particle Green function. Using a matrix notation with respect to $\mathbf{L} = \{L_1, L_2\}$ and \mathbf{L}' , the two-particle Green function reads as

$$\mathbf{G}_{i_c \sigma \sigma_c}^{(2)}(E) = \mathbf{G}_{i_c \sigma \sigma_c}^{(2,0)}(E) \left(1 - \mathbf{U} \mathbf{G}_{i_c \sigma \sigma_c}^{(2,0)}(E)\right)^{-1} \quad (34)$$

with $U_{\mathbf{L} \mathbf{L}'} = U_{L_1 L_2 L_1' L_2'}$. $G_{i_c \sigma \sigma_c}^{(2,0), \mathbf{L} \mathbf{L}'}(E)$ is the two-particle Green function which has to be calculated from the self-

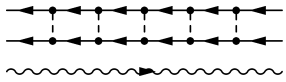


FIG. 4: Typical diagram of the VV ladder. Solid line: renormalised valence-band propagator. Wiggly line: core-propagator. Dashed line: VV interaction.

convolution of the partial QDOS

$$\begin{aligned} A_{i_c \sigma \sigma_c}^{(2,0), \mathbf{L} \mathbf{L}'}(E) &= \delta_{\mathbf{L} \mathbf{L}'} \int dE' \rho_{i_c \sigma}^{L_1}(E - E') \rho_{i_c \sigma_c}^{L_2}(E') \\ &\quad \times (f_-(E' - E) f_-(-E') - f_-(E - E') f_-(E')) \end{aligned} \quad (35)$$

using the spectral representation:

$$G_{i_c \sigma \sigma_c}^{(2,0), \mathbf{L} \mathbf{L}'}(E) = \int dE' \frac{A_{i_c \sigma \sigma_c}^{(2,0), \mathbf{L} \mathbf{L}'}(E')}{E - E'}. \quad (36)$$

In equation (34) we have applied the local approximation, i. e. only the on-site elements for $i = i_c$ are assumed to be non-zero. This approximation is analogous to the local approximation for the one-particle Green function in section IV.

B. VV and CV correlations

A straightforward way to include the direct CV correlation on the same level as the direct VV correlations has been discussed in Refs. 35,36,37,38. This leads to the (“three-particle”) CVV ladder approximation. For the limiting case of completely filled or empty bands the CVV ladder represents the exact solution and recovers the VV ladder but shifted energetically by $2U_c$ due to the CV interaction¹⁸. A typical diagram is shown in figure 5 where the dotted line represents the CV interaction. The CVV ladder approximation leads to a coupled set of Fredholm integral equations¹⁸. For a multi-band model, however, the numerical evaluation is beyond our present computational capacities. We therefore discuss a simpler approximation where only diagrams up to first order in the direct correlations are retained (see figure 6).

C. Results for Ni

The calculated Auger spectra for Ni resulting from different approximations are shown in figure 7. The core hole is assumed to be unpolarised (non-resonant⁶¹ process). The intensities for core spin σ_c and $-\sigma_c$ are added incoherently: $I_\sigma(E) = (I_{\sigma \sigma_c}(E) + I_{\sigma -\sigma_c}(E))/2$. However, the Auger intensity is still spin-dependent due to the ferromagnetic order in Ni.

In figure 7 we plotted the total Auger-intensity $I_\uparrow(E) + I_\downarrow(E)$ on the left and the spin asymmetry $(I_\uparrow(E) - I_\downarrow(E))/(I_\uparrow(E) + I_\downarrow(E))$ on the right. Part (a) shows the

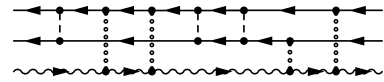


FIG. 5: Typical diagram in the CVV ladder approximation. The notation is the same as in figure 4. The additional CV interaction is represented by the dotted line.

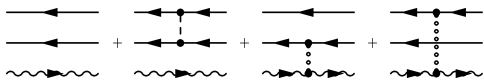


FIG. 6: Diagrams up to first order in the VV and CV interaction (notation as in figure 5).

result of the self-convolution model (equations (33) and (35) inserted in (31)), i. e. the self-convolution of the occupied QDOS in figure 1 (l. h. s.). Direct correlations and core-hole screening are neglected altogether. Part (b) corresponds to the VV ladder approximation starting from the (unscreened) QDOS. Taking additionally into account the screening effects introduced by the presence of the core hole in the initial state results in (c). The spectrum obtained by the first order in the direct VV and CV correlations (see figure 6) and by the screened QDOS is plotted in part (d).

As one can see in the plots on the left-hand side, the VV interaction is too weak to produce bound states, no sharp satellite appears, and the spectra appear to be band-like. Compared to the self-convolution (a), however, a considerable shift to lower energies is observed in (b). This shift results from the direct correlations between the two final-state holes in the valence band. In (c) the main peak is shifted to still lower energies. This is an effect of the core-hole screening in the initial state and can be traced back to the redistribution of spectral weight in the screened QDOS (figure 1). Compared to (a) and (b), the total AES intensity is clearly increased in (c). Again this is a consequence of the core-hole screening since the number of occupied states available for the Auger process is increased (figure 1, r. h. s.). The spectrum shown in (d) not only includes the initial-state core-hole screening but the final-state effects due to the destruction of the core hole. Compared to (c), where the initial state is described in the same way, these effects result in a strong shift of the main peak to higher energies. This shift almost exactly compensates the shifts to lower energies that are due to direct VV correlations (b) and the core-hole screening (c). However, a weak shoulder at about $E = -8.5$ eV remains in the spectrum (d).

In all cases there is a high spin asymmetry (up to -50%) for energies between approximately -0.8 eV and 0. This is a consequence of the fact that Ni is a strong ferromagnet. There are almost no \uparrow -electrons above about -0.4 eV (see figure 1) that can participate in the Auger-process. The main contribution to the intensity is therefore due to triplet configurations where the two final-state holes or, equivalently, core-hole and Auger electron have spin \downarrow . However, the intensity is very small in this energy region. By taking into account the screening of the core hole in the initial state (compare (b) and (c)) the spin asymmetry is reduced over the whole energy range which essentially is the same effect as the reduction of the local magnetic moment at i_c caused by the presence of the

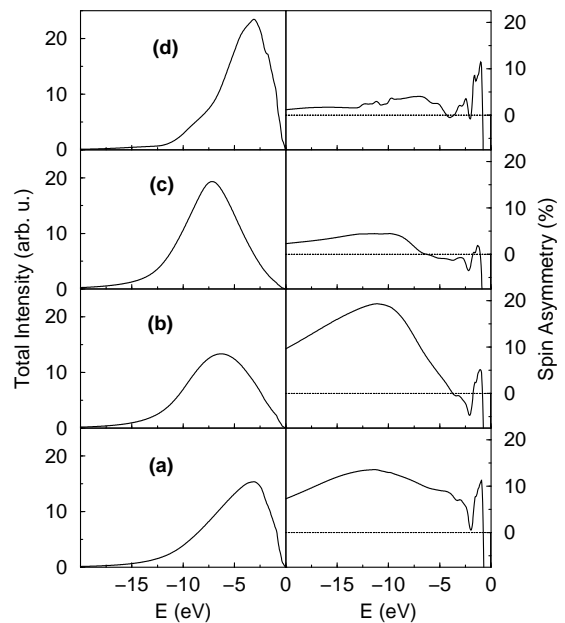


FIG. 7: Left: total intensities $I_{\uparrow}(E) + I_{\downarrow}(E)$. Right: spin-asymmetry $(I_{\uparrow}(E) - I_{\downarrow}(E))/(I_{\uparrow}(E) + I_{\downarrow}(E))$. (a) self-convolution without screening of the core hole in the initial state; (b) VV ladder without core hole screening; (c) screened VV ladder; (d) direct VV and CV correlations included up to first order (figure 6).

core hole (figure 3). The total spin-polarisation

$$P = \frac{\int dE I_{\uparrow}(E) - \int dE I_{\downarrow}(E)}{\int dE I_{\uparrow}(E) + \int dE I_{\downarrow}(E)} \quad (37)$$

in the case (d) is 2.6% and 1.6% for (c). Both values are close to the experimental value⁶¹ of 2% for the $M_1M_{45}M_{45}$ -process. The cases (a) and (b) with a polarisation of 8.7% and 9.3%, respectively, overestimate the total spin-polarisation compared with the experimental value.

For the calculation of the orbitally resolved contributions to the Auger intensity we may restrict the summation in equation (31) to orbital indices (L_1, L_2, L'_1, L'_2) belonging to $t_{2g}(e_g)$ -character only. The resulting contributions are shown on the left (right) of figure 8. The contributions due to the remaining terms are plotted in the middle.

In all cases (a)–(b) the t_{2g} contributions are clearly stronger compared with the e_g contributions. The ratio between the t_{2g} and e_g partial intensities corresponds to the different degeneracies. Comparing the cases (a)–(d), we notice that there are essentially the same trends in the partial intensities as for the total intensities, and the discussion is the same as above. The line shape in case (d), however, shows up some fine structure, especially in the t_{2g} partial intensity, which is not that pronounced in the total intensity. The shoulder at the low-energy tail of (d) is due to direct VV correlations and may be inter-

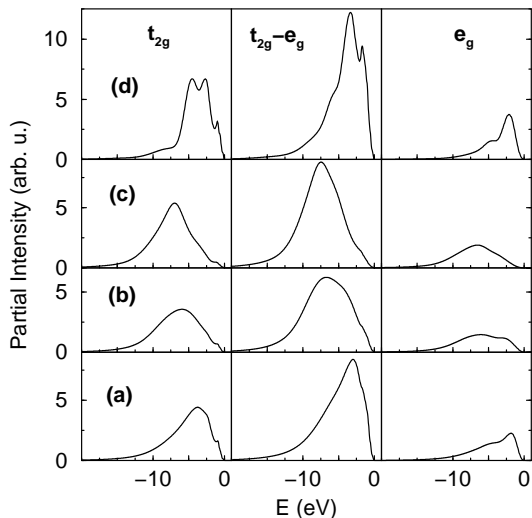


FIG. 8: Contributions to the total Auger intensity (figure 7) of processes involving t_{2g} -electrons only (left), e_g -electrons only (right) and both kinds of d-electrons (middle).

preted as a hint for the formation of a bound state of the final holes. Except for this shoulder, a surprising similarity between (d) and (a) is noticed, even for the orbital resolved spectra. This might also be due to the small number of diagrams taken into account. However, the cancellation of effects according to different interactions (VV and CV) was also pointed out in Ref. 27.

VI. SUMMARY

In this paper we have investigated electron-correlation effects on the Auger line shape of Ni as an example of a ferromagnetic 3d-transition metal. The starting point is a realistic set of hopping and overlap parameters taken from tight-binding band-structure calculations. We additionally consider a strongly screened on-site Coulomb interaction between the rather localised 3d electrons. The respective Coulomb-matrix elements are expressed in terms of effective Slater integrals. Choosing a non-orthogonal basis, a distinction between the different angular-momentum characters of the valence orbitals is possible. This is necessary for the precise definition of the Coulomb-interaction part in the (multi-band Hubbard) Hamiltonian and also facilitates the interpretation of the Auger spectra. Furthermore, we account for the core-valence interaction which is responsible for the screening of the core hole in the initial state of AES and for the sudden response of the valence electrons due to the destruction of the core hole in the final state.

Within a diagrammatic approach, the indirect and the direct correlations can be studied separately. The indirect correlations have been treated by second-order perturbation theory around the Hartree-Fock solution

(SOPT-HF). The VV interaction parameters are fixed by assuming a ratio $J/U \approx 0.2$ and by fitting the experimentally observed magnetic moment for $T = 0$ K, leading to $U = 2.47$ eV and $J = 0.5$ eV. This is equivalent to an intra-orbital interaction of $U_{LLLL} = 3.07$ eV ($L = \{2, m_2\}$). The resulting Curie temperature within the theory presented here is by a factor 2.6 larger than the experimentally observed one but considerably lower than the LDA+ U (Hartree-Fock) value.

The core-valence interaction leads to a breakdown of the translational invariance in the initial state for AES. The interaction parameter $U_c = 1.81$ eV is fixed by requiring charge neutrality at the site i_c where the core hole is created. The screening of the additional core-hole potential causes a transfer of spectral weight below the Fermi energy and thus a considerable reduction of the local magnetic moment. However, the local magnetic moment is finite since the s- and p-electrons also contribute to the screening.

To study the direct correlations we have used two different approaches. The first is the VV ladder approximation, which results in a band-like Auger spectrum with a single maximum. In a second approach we have summed up the first-order diagrams with respect to the VV and CV interaction. The resulting spectrum shows up a shoulder at the lower tail due to the VV interaction. Otherwise the line shape is very similar to that obtained by the self-convolution of the unscreened QDOS.

As far as concerns the line shape, we conclude that the different correlation effects, VV and CV correlations in the initial and the final state, nearly cancel. However, a strong effect of electron correlations has been found in the orbitally resolved partial intensities and particularly for the spin-asymmetry.

The calculated spin polarisation is in a good agreement with the measured one of the $M_1M_{45}M_{45}$ -process⁶¹. This corresponds to the excitation of a not too deep lying core level, i. e. the two-step model should be applicable. The reduced but finite spin polarisation of the $M_1M_{45}M_{45}$ -process (as compared to the band polarisation) can be explained by effects of core-hole screening rather than by a core-hole polarisation, caused by a resonant excitation of the core electron into the valence band⁶¹. Future work will show whether these findings also apply to other 3d-transition metals.

Acknowledgments

Financial support of the *Deutsche Forschungsgemeinschaft* within the project No. 158/5-1 is gratefully acknowledged. The numerical calculations were performed on the CrayT3E at the *Konrad-Zuse-Zentrum für Informationstechnologie Berlin (ZIB)*.

APPENDIX A: NON-ORTHOGONAL BASIS-SET

There are several advantages for using the non-orthogonal basis set $\{|iL\sigma\rangle\}$. The Slater-Koster parameters⁶² for the two-center approximation (used here) are much more accurate for a non-orthogonal basis set compared to an orthonormal one⁴². Secondly, the non-orthogonal basis (LCAO basis) is built up from quasi-atomic orbitals. One therefore knows the behaviour of the basis states under symmetry operations belonging to the O_h -group which eventually results in the fact that local quantities, e.g. the on-site Green function, are diagonal in the orbital index. Furthermore, the Coulomb matrix elements can be calculated in a highly symmetric way by using $3j$ -symbols in combination with a transformation from spheric to cubic harmonics. The unknown radial parts of the basis are parametrised by the effective Slater integrals (F^0 , F^2 , F^4). Finally, one can ensure that the Coulomb interaction acts between 3d-electrons only.

For the formalism of second quantisation, for the many-body and Green-function theory, for the proof of Wick's theorem and thus the development of the diagram technique, however, the use of an orthonormal set of one-particle basis states is necessary. Therefore, it is convenient to derive all expressions that refer to the non-orthogonal basis,

$$\langle\alpha|\beta\rangle = S_{\alpha\beta}, \quad (\text{A.1})$$

by a (non-unitary) Löwdin transformation⁶³ from a related set of orthogonal one-particle basis states:

$$|\tilde{\alpha}\rangle \stackrel{\text{Def.}}{=} \sum_{\beta} |\beta\rangle S_{\beta\alpha}^{-1/2}. \quad (\text{A.2})$$

The overlap matrix \mathbf{S} is Hermitian, $\{|\tilde{\alpha}\rangle\}$ indeed represents an orthonormal and complete basis set. The completeness relation can be written as

$$\begin{aligned} 1 &= \sum_{\alpha} |\tilde{\alpha}\rangle\langle\tilde{\alpha}| = \sum_{\alpha\beta\gamma} |\beta\rangle S_{\beta\alpha}^{-1/2} S_{\alpha\gamma}^{-1/2} \langle\gamma| \\ &= \sum_{\alpha\beta} |\alpha\rangle S_{\alpha\beta}^{-1} \langle\beta|. \end{aligned} \quad (\text{A.3})$$

Annihilation (and creation) operators referring to the non-orthogonal basis may be defined as:

$$c_{\alpha} \stackrel{\text{Def.}}{=} \sum_{\beta} S_{\alpha\beta}^{-1/2} \tilde{c}_{\beta}. \quad (\text{A.4})$$

It is instructive to see how the creation operator acts on the vacuum state:

$$\begin{aligned} c_{\alpha}^{\dagger}|0\rangle &= \sum_{\beta} \tilde{c}_{\beta}^{\dagger} S_{\beta\alpha}^{-1/2}|0\rangle = \sum_{\beta} |\tilde{\beta}\rangle S_{\beta\alpha}^{-1/2} \\ &= \sum_{\beta\gamma} |\gamma\rangle S_{\gamma\beta}^{-1/2} S_{\beta\alpha}^{-1/2} = \sum_{\beta} |\beta\rangle S_{\beta\alpha}^{-1}. \end{aligned} \quad (\text{A.5})$$

Furthermore, one gets from the transformations (A.2) and (A.4):

$$\sum_{\alpha} |\tilde{\alpha}\rangle \tilde{c}_{\alpha} = \sum_{\alpha\beta\gamma} |\beta\rangle S_{\beta\alpha}^{-1/2} S_{\alpha\gamma}^{1/2} c_{\gamma} = \sum_{\alpha} |\alpha\rangle c_{\alpha}. \quad (\text{A.6})$$

Thus, an operator in second quantisation has the same structure for both, the orthonormal and the non-orthogonal basis set. A one-particle operator O , for example, reads as:

$$\begin{aligned} O &= \sum_{\alpha,\alpha'} \tilde{c}_{\alpha}^{\dagger} \langle\tilde{\alpha}|o|\tilde{\alpha}'\rangle \tilde{c}_{\alpha'} \\ &\stackrel{(\text{A.6})}{=} \sum_{\alpha,\alpha'} c_{\alpha}^{\dagger} \langle\alpha|o|\alpha'\rangle c_{\alpha'}. \end{aligned} \quad (\text{A.7})$$

The non-orthogonal Green functions are defined as in the orthonormal case, e.g. $G_{\alpha\alpha'}(E) = \langle\langle c_{\alpha}; c_{\alpha'}^{\dagger} \rangle\rangle$ for the one-particle Green function. For example, using the non-orthogonal version of the fundamental anti-commutation rules ($[c_{\alpha}, c_{\alpha'}^{\dagger}]_{+} = S_{\alpha\alpha'}^{-1}$, see also Eq. (4)) and the equation of motion, the non-interacting Green function turns out to be:

$$\mathbf{G}^0(E) = ((E + \mu)\mathbf{S} - \mathbf{T})^{-1} \quad (\text{A.8})$$

where we used the matrix notation $(\mathbf{G})_{\alpha\alpha'} = G_{\alpha\alpha'}$ etc. For the interacting Green function one has (compare with Eq. (15)):

$$\mathbf{G}(E) = ((E + \mu)\mathbf{S} - \mathbf{T} - \Sigma(E))^{-1}. \quad (\text{A.9})$$

In the same way as for the examples given, one may use Wick's theorem, develop the diagram technique etc.

* torsten.wegner@physik.hu-berlin.de

¹ J. C. Fuggle, *Electron Spectroscopy: Theory, Techniques and Applications* (Academic, London, 1981), vol. 4, p. 85.

² R. Weissmann and K. Müller, *Surf. Sci. Rep.* **105**, 251 (1981).

³ C.-O. Almbladh and L. Hedin, *Handbook on Synchrotron Radiation* (North-Holland, Amsterdam, 1983), vol. 1b, p. 607.

⁴ P. Weightman, *Electronic Properties of surfaces* (Adam Hilger, Bristol, 1984), p. 135.

- ⁵ S. B. Whitefield, G. B. Armen, R. Carr, J. C. Levin, and B. Crasemann, *Phys. Rev. A* **37**(2), 419 (1988).
- ⁶ D. D. Sarma, C. Carbone, P. Sen, and W. Gudat, *Phys. Rev. B* **40**(18), 12542 (1989).
- ⁷ D. E. Ramaker, *Crit. Rev. Solid State Mater.* **17**, 211 (1991).
- ⁸ D. D. Sarma, S. R. Barman, R. Cimino, C. Carbone, P. Sen, A. Roy, A. Chainani, and W. Gudat, *Phys. Rev. B* **48**(10), 6822 (1993).
- ⁹ J. J. Lander, *Phys. Rev.* **91**, 1382 (1953).
- ¹⁰ C. J. Powell, *Phys. Rev. Lett.* **30**, 1179 (1973).
- ¹¹ G. Hörmandinger, P. Weinberger, P. Marksteiner, and J. Redinger, *Phys. Rev. B* **38**(2), 1040 (1988).
- ¹² Y. Kucherenko and P. Rennert, *J. Phys.: Condens. Matter* **9**, 5003 (1997).
- ¹³ M. Cini, *Solid State Commun.* **24**, 681 (1977).
- ¹⁴ G. A. Sawatzky, *Phys. Rev. Lett.* **39**(8), 504 (1977).
- ¹⁵ G. A. Sawatzky and A. Lenseink, *Phys. Rev. B* **21**(5), 1790 (1980).
- ¹⁶ M. Cini, *Phys. Rev. B* **17**(6), 2788 (1978).
- ¹⁷ W. Nolting, G. Geipel, and K. Ertl, *Phys. Rev. B* **45**(11), 5790 (1992).
- ¹⁸ M. Potthoff, J. Braun, W. Nolting, and G. Borstel, *J. Phys.: Condens. Matter* **5**, 6879 (1993).
- ¹⁹ W. Nolting, W. Borgiel, V. Dose, and T. Fauster, *Phys. Rev. B* **40**(7), 5015 (1989).
- ²⁰ W. Nolting, A. Vega, and T. Fauster, *Z. Phys. B* **96**, 357 (1995).
- ²¹ M. Potthoff, T. Wegner, and W. Nolting, *Phys. Rev. B* **55**, 16132 (1997).
- ²² H. Kajueter and G. Kotliar, *Int. J. Mod. Phys. B* **11**, 729 (1997).
- ²³ A. I. Lichtenstein and M. I. Katsnelson, *Phys. Rev. B* **57**(12), 6884 (1998).
- ²⁴ K. Held and D. Vollhardt, *Eur. Phys. J. B* **5**(3), 473 (1998).
- ²⁵ W. Metzner and D. Vollhardt, *Phys. Rev. Lett.* **62**, 324 (1989).
- ²⁶ M. I. Katsnelson and A. I. Lichtenstein, *J. Phys.: Condens. Matter* **11**, 1037 (1999).
- ²⁷ D. D. Sarma and P. Mahadevan, *Phys. Rev. Lett.* **81**(8), 1658 (1998).
- ²⁸ V. Drchal, *J. Phys.: Condens. Matter* **1**, 4773 (1989).
- ²⁹ M. Kotrla and V. Drchal, *J. Phys.: Condens. Matter* **4**, 4251 (1992).
- ³⁰ M. Cini, *Surf. Sci.* **87**, 483 (1979).
- ³¹ G. Tréglia, M. C. Desjonquères, F. Ducastelle, and D. Spanjaard, *J. Phys. C* **14**, 4347 (1981).
- ³² V. Drchal and J. Kudrnovský, *J. Phys. F* **14**, 2443 (1984).
- ³³ W. Nolting, *Z. Phys. B* **80**, 73 (1990).
- ³⁴ W. Nolting, G. Geipel, and K. Ertl, *Phys. Rev. B* **44**(22), 12197 (1991).
- ³⁵ M. Potthoff, J. Braun, G. Borstel, and W. Nolting, *Phys. Rev. B* **74**(19), 12480 (1993).
- ³⁶ M. Potthoff, J. Braun, and G. Borstel, *Z. Phys. B* **95**, 207 (1994).
- ³⁷ M. Potthoff, J. Braun, W. Nolting, and G. Borstel, *Surf. Sci.* **307-309**, 942 (1994).
- ³⁸ M. Potthoff, J. Braun, G. Borstel, and W. Nolting, *J. Electron Spectrosc. Rel. Phen.* **72**, 163 (1995).
- ³⁹ A. A. Abrikosov, L. P. Gorkov, and I. E. Dzyaloshinski, *Methods of Quantum Field Theory in Statistical Mechanics* (Dover, New York, 1975).
- ⁴⁰ L. Kleinman and K. Mednick, *Phys. Rev. B* **24**(12), 6880 (1981).
- ⁴¹ M. M. Steiner, R. C. Albers, and L. J. Sham, *Phys. Rev. B* **45**(23), 13272 (1992).
- ⁴² D. A. Papaconstantopoulos, *Handbook of the band structure of elemental solids* (Plenum, New York, 1986).
- ⁴³ S. Sugano, Y. Tanabe, and H. Kamimura, *Multiplets of transition-metal ions in crystals*, vol. 33 of *Pure and applied physics* (Academic, New York, 1970).
- ⁴⁴ V. I. Anisimov, F. Aryasetiawan, and A. I. Lichtenstein, *J. Phys.: Condens. Matter* **9**, 767 (1997).
- ⁴⁵ D. N. Zubarev, *Sov. Phys. Uspekhi* **3**, 320 (1960).
- ⁴⁶ W. Nolting, *Vielteilchentheorie*, vol. 7 of *Grundkurs: Theoretische Physik* (Zimmermann-Neufang, Ulmen, 1995).
- ⁴⁷ H. Schweitzer and G. Czycholl, *Z. Phys. B* **83**, 93 (1991).
- ⁴⁸ M. Potthoff and W. Nolting, *Z. Phys. B* **104**, 265 (1997).
- ⁴⁹ P. Lambin and J. P. Vigneron, *Phys. Rev. B* **29**(6), 3430 (1984).
- ⁵⁰ V. I. Anisimov, A. I. Poteryaev, M. A. Korotin, A. O. Anokhin, and G. Kotliar, *J. Phys.: Condens. Matter* **9**, 7359 (1997).
- ⁵¹ S. Hirooka and M. Shimizu, *Phys. Lett.* **46A**, 209 (1973).
- ⁵² M. Fleck, A. M. Oleś, and L. Hedin, *Phys. Rev. B* **56**(6), 3159 (1997).
- ⁵³ C. Guillot, Y. Ballu, J. Paigne, J. Lecante, K. P. Jain, P. Thiry, R. Pinchaux, Y. Petroff, and L. M. Falicov, *Phys. Rev. Lett.* **39**, 1632 (1977).
- ⁵⁴ Y. Sakisaki, T. Komeda, M. Ouchi, H. Kato, S. Masuda, and K. Yagi, *Phys. Rev. Lett.* **58**, 733 (1987).
- ⁵⁵ S. Raaen and V. Murgai, *Phys. Rev. B* **36**, 887 (1987).
- ⁵⁶ A. Liebsch, *Phys. Rev. B* **23**(10), 5203 (1981).
- ⁵⁷ V. Drchal, V. Janiš, and J. Kudrnovský, *cond-mat/9810181* (1998), <http://xxx.lan.gov/abs/>.
- ⁵⁸ P. J. Brown, J. Deportes, and K. R. A. Ziebeck, *J. Phys. I France* **1**, 1529 (1991).
- ⁵⁹ P. J. Brown, J. Deportes, K. U. Neumann, and K. R. A. Ziebeck, *J. Magn. Magn. Mat.* **104-107**, 2083 (1992).
- ⁶⁰ M. B. Stearns, *Landolt-Börnstein, New Series* (Springer, Berlin, 1984), vol. 19a of *Group III*, chap. Magnetic Properties of Metals.
- ⁶¹ R. Allenspach, D. Mauri, M. Taborelli, and M. Landolt, *Phys. Rev. B* **35**(10), 4801 (1987).
- ⁶² J. C. Slater and G. F. Koster, *Phys. Rev.* **94**(6), 1498 (1954).
- ⁶³ P.-O. Löwdin, *J. Chem. Phys.* **18**(3), 365 (1950).